Continental Shelf Research 28 (2008) 2668–2677

Contents lists available at ScienceDirect

Continental Shelf Research

journal homepage: www.elsevier.com/locate/csr

Modeling flocculation processes of fine-grained particles using a size-resolved method: Comparison with published laboratory experiments

Fanghua Xu *, Dong-Ping Wang, Nicole Riemer [1]

School of Marine and Atmospheric Sciences, Stony Brook University, Stony Brook, NY, USA

ARTICLE INFO

Article history:
Received 4 April 2008
Received in revised form
5 August 2008
Accepted 10 September 2008
Available online 16 September 2008

Keywords:
Flocculation
Fine-grained sediment
Numerical simulation

ABSTRACT

The transport of fine-grained particles in estuarine and coastal waters is influenced by flocculation processes (aggregation and floc breakup). As a consequence, the particle size varies with time in the water column, and can be orders of magnitude larger than those of primary particles. In this study the variations in floc size is simulated using a size-resolved method, which approximates the real size distribution of particles by a range of size bins and solves a mass balance equation for each bin. To predict the size distribution both aggregation and breakup processes are included. The conventional rectilinear aggregation kernel is used which considers both turbulent shear and differential settling. The breakup kernel accounts for the fractal dimension of the flocs. A flocculation simulation is compared to the settling column lab experiments of Winterwerp [1998. A simple model for turbulence induced flocculation of cohesive sediment, Journal of Hydraulic Research, 36, 309–326], and a one-dimensional sediment transport model is verified with the observed variations in floc size and concentration over tidal cycles in a laboratory flume experiment of Bale et al. [2002. Direct observation of the formation and break-up of aggregates in an annular flume using laser reflectance particle sizing. In: Winterwerp, J.C., Kranenburg, C. (Eds.), Fine Sediment Dynamics in the Marine Environment. Elsevier, pp. 189–201]. The numerical simulations compare qualitatively and quantitatively well with the laboratory measurements, and the analysis of the two simulation results indicates that the median floc size can be correlated to the sediment concentration and Kolmogorov microscale. Sensitivity studies are conducted to explore the role of settling velocity and erosion rate. The results are not sensitive towards the formulation of settling velocity, but the parameterization of erosion flux is important. The studies show that for predicting the sediment deposition flux it is crucial to include flocculation processes.

1. Introduction

Suspended fine-grained sediments ($<63\,\mu m$) in estuaries often exist in the form of flocs (Eisma et al., 1994). Flocs are capable of adsorbing organic carbon, nutrients and anthropogenic contaminants (Syvitski et al., 1995). Thus, they play a key role in the transport of the suspended matter to the bottom. The main difficulties in predicting the fate and transport of the suspended matter are the spatial and temporal variations in the floc size and hence their settling velocity (Mikkelsen et al., 2005). The floc size can vary from a few micrometers to hundreds, even thousands of micrometers (Hill et al., 1998; Fugate and Friedrichs, 2003; Traykovski et al., 2004; Uncles et al., 2006). Typically, large flocs sink much faster than their component grains. The variations in floc size are primarily due to flocculation processes, such as aggregation and breakup. A better understanding of these processes is critical to predict the transport of fine-grained sediments.

Flocculation is affected by many factors, including suspended sediment concentration (SSC), turbulence-induced shear, differential settling of flocs and sticky organic matter in the water column (Dyer and Manning, 1999; Geyer et al., 2004). The individual contribution of these factors to the floc size is unclear. The floc growth rate appears to depend on SSC in a nonlinear way. Kranck and Milligan (1992) found that the floc size increases with increasing SSC. However, the floc size is not always positively correlated with SSC. For example, Hill et al. (2000) found that the floc size was uniform despite a wide variability in concentration. They suggested that highly turbid water might limit floc growth. Turbulence can increase particle collisions and form flocs; on the other hand, turbulent shear may tear large floc apart and limit

* Corresponding author. Tel.: +1 631 889 0232.
E-mail address: fhxu2005@hotmail.com (F. Xu).
[1] Now at the Department of Atmospheric Sciences, University of Illinois at Urbana-Champaign, Urbana, Illinois.

0278-4343/$ - see front matter © 2008 Elsevier Ltd. All rights reserved.
doi:10.1016/j.csr.2008.09.001

maximal floc size under energetic conditions (Hunt, 1986). Under low-to-moderate energy environments, the floc size is possibly controlled by forces exerted on sinking flocs by the relative particle–fluid motion (Hill et al., 2001). Differential settling describes the process that large particles sink faster than smaller ones and may capture the small particles during settling. Sticky organic matter in the water column affects the particle stickiness, that is, the probability that two particles will adhere once they have collided, which has a large natural variability, ranging from $O(10^{-3})$ to $O(1)$ (Hill and Nowell, 1995).

The importance and complexity of particle aggregation have triggered numerous numerical modeling in various fields of the atmospheric sciences, environmental sciences and in engineering. Smoluchowski (1917) originally proposed a coagulation equation for particles colliding due to Brownian motion. After that other physical mechanisms, such as shear and differential settling, have been proposed to influence the particle size distribution (Pruppacher and Klett, 1980). Regarding the coagulation in open ocean environments, Farley and Morel (1986) numerically solved the coagulation equation for a single pulse input of colloidal particles (size $<1\,\mu m$) in a well-mixed (zero dimension) system by assuming spherical particles with constant density. Burd and Jackson (1997) updated the model of Farley and Morel (1986) by including effects of fractal structure and hydrodynamic interaction. Their study shows that the fractal structure alters the floc density and settling velocity, and the simulation results are sensitive to the variations in fractal dimension. On the other hand, the hydrodynamic deflection of particles around each other does not have a significant impact.

Sediment transport models involving flocculation processes are few (Lavelle, 1993). A 'characteristic' settling velocity for flocs is commonly used for simulation of SSC profiles (e.g., Orton and Kineke, 2001; Warner et al., 2005). The merit of this approach is that only one parameter needs to be calibrated. Power law parameterizations are also widely used to describe variations in settling velocity with SSC. However, the parameters for the power law can vary considerably from site to site (Spearman and Roberts, 2002). Power law with dissipation parameter function, which includes the effect of increasing turbulence on floc breakup, was suggested by van Leussen (1994). A simple flocculation model incorporating turbulence-induced growth and breakup of flocs was proposed by Winterwerp (1998). The model estimates the equilibrium median floc size and applies a fractal treatment to modify the Stokes' law relating settling velocity to floc size. The flocculation model was implemented in a three-dimensional hydrodynamic model to simulate the turbidity maximum in the Ems estuary (Winterwerp, 2002). These model studies have clearly demonstrated the importance of including flocculation processes in sediment transport models.

The objective of this study is to develop a flocculation model which explicitly predicts the particle size and concentration distributions in estuarine and coastal environments. In Section 2, we simulate flocculation processes using a size-resolved method which is mass-conserved and computationally efficient. The flocculation simulation is compared with published laboratory observations. Both aggregation and breakup processes are included, considering the effects of turbulent shear. The breakup kernel calculation accounts for the fractal dimension of the flocs. Sensitivity tests are performed to inspect the influence of fractal dimension and particle stickiness. Section 3 presents a one-dimensional (1-D) sediment transport model and the comparison of the simulation results with laboratory observations published in the current literature. We also explore the sensitivity of the model towards model parameters like the parameterizations of settling velocity and erosion rate. Section 4 concludes our findings.

2. Flocculation

Our size-resolved method for understanding flocculation of sediment particles is based on the Smoluchowski framework. This framework considers mass conservation for particles in different size bins, which approximates the real size distribution of particles. For each bin, a balance equation for the mass density is solved. A basic form of the equation is (Hill and Nowell, 1995; Bott, 1998):

$$\frac{\partial n(m,t)}{\partial t} = \frac{1}{2}\int_{m_0}^{m} n(m_c,t)K(m_c,m')n(m',t)\,dm' - \int_{m_0}^{\infty} n(m,t)K(m,m')n(m',t)\,dm' + \int_{m_0}^{\infty} Q(m,m')P(m')n(m',t)\,dm' - n(m,t)P(m), \quad (1)$$

where $n(m,t)$ is the particle number density as a function of time t and mass m, m_0 is the mass of particle in the first bin, $K(m_c,m')$ is the aggregation kernel describing the rate of particle contacts ($m_c = m-m'$), $P(m)$ is the breakup kernel due to turbulent shear, and $Q(m,m')$ represents the number density function for the fragments formed by the breakup of a parent particle of mass m'. The integrals on the right hand side of Eq. (1) represent: the gain rate of particles of mass m by collision of two smaller particles; the loss of particles with mass m due to collision with other particles; the number increase of particles with mass m from breakup of larger flocs; and the loss of particles with mass m due to breakup.

Theoretical and numerical investigations on floc breakup dynamics have been reported in the literature (Spicer and Pratsinis, 1996; Zhang and Li, 2003; Maggi, 2005), but experimental data are rare. Three distinct breakage distribution functions, binary, ternary and Gaussian distribution, were proposed by Spicer and Pratsinis (1996). Numerical experiments by Zhang and Li (2003) showed no significant differences in the results of the steady-state size distributions from the three breakage functions. The simplest binary breakup is used in the present study. $Q(m,m')$ is defined as (Zhang and Li, 2003):

$$Q(m,m') = \begin{cases} 2 & (m = m'/2) \\ 0 & (m \neq m'/2). \end{cases} \quad (2)$$

The breakup kernel, P, is a function of shear rate and floc size. The flocs are considered to be composed of primary particles. Assuming a fractal treatment, the breakup frequency can be written as (Winterwerp, 1998):

$$P_i = E\sqrt{\frac{\mu}{F_y}}G^{1.5}(2r_i)\left(\frac{r_i - r_1}{r_1}\right)^{3-n_f}, \quad (3)$$

where μ is the dynamic viscosity, n_f is the fractal dimension, and $F_y \approx 10^{-10}$ Pa is the estimated yield strength. The fractal dimension of flocs is defined as (Winterwerp, 2002)

$$n_f = \lim_{L\to\infty}\frac{\ln(N(L))}{\ln(L)}, \quad (4)$$

where $N(L)$ is the number of self similar primary particles and L is the linear particle size. The typical value of n_f varies from about 1.4 for fragile flocs to about 2.2 for strong estuarine flocs (Winterwerp, 1998). $n_f = 2$ is applied in calculating breakup kernel.

The aggregation is due to turbulent shear and differential settling. Brownian motion is neglected because it is only important when the particle size is less than 1 μm (Winterwerp, 2002). The concentration of particles of this size is negligible in estuaries. The rectilinear aggregation kernel is $K = \alpha(K_{ts}+K_{ds})$ (Burd and Jackson, 1997), where α is the particle stickiness, and

the kernels K_{ts} and K_{ds} estimate the collision rate per unit volume caused by turbulence shear and differential settling (Hill et al., 2001). Specifically, the kernels K_{ts} and K_{ds} are given by:

$$K_{ts} = \tfrac{4}{3}G(r_i + r_j)^3 \tag{5}$$

and

$$K_{ds} = \pi \cdot (r_i + r_j)^2 \cdot |w_{s,i} - w_{s,j}|, \tag{6}$$

where r_i and r_j are the floc radius, $w_{s,i}$ and $w_{s,j}$ are the settling velocity of flocs in bin i and j. The shear rate is defined as $G = \sqrt{\varepsilon/\nu}$, where ε is the turbulent dissipation rate and ν is the kinematic viscosity of fluid. The settling velocity is calculated as a function of particle size from Sternberg et al. (1999),

$$w_{s,j} = 347.5602(2r_j)^{1.54}, \tag{7}$$

where r_j is in m, and $w_{s,j}$ is in $\mathrm{m\,s^{-1}}$. Eq. (7) is an empirical relationship obtained by the regression between measured size and settling velocity of suspended flocs. It incorporates the effects of variable floc densities due to the fractal structure. Substituting Eq. (7) into the Stokes' Law, the floc effective density $\Delta\rho = \rho_{floc} - \rho_{water}$ can be estimated as a function of floc size, i.e., $\Delta\rho \propto D^{-0.46}$. Sternberg et al. (1999) found their results comparable with several other measurements with the exponent between $\Delta\rho$ and floc size varying from -1.40 to -0.46. The effect of fractal structure of flocs is implicitly included in Eq. (7). The differential settling kernel (Eq. (6)) is further multiplied by a factor of 5 to include the fact that irregular floc shapes can increase the efficiency of floc contacts. The empirical factor 5 is selected, which best fits the lab flume experiment.

For the numerical solution of Eq. (1) we use the flux method by Bott (1998), which has been successfully used in predicting the coagulation of cloud droplets (Riemer and Wexler, 2005). We introduce the mass density function $g(y,t)$ by

$$g(y,t)\,\mathrm{d}y = mn(m,t)\,\mathrm{d}m,$$
$$n(m,t) = \frac{1}{3m^2}g(y,t) \tag{8}$$

where $y = \ln r$ and r is the radius of flocs with mass m. When Eq. (8) is substituted into Eq. (1), a balance equation for the mass density is obtained:

$$\begin{aligned}\frac{\partial g(y,t)}{\partial t} = {} & \frac{1}{2}\int_{y_0}^{y}\frac{m^2}{m_c^2 m'}g(y_c,t)K(y_c,y')g(y',t)\,\mathrm{d}y' \\ & - \int_{y_0}^{\infty}\frac{1}{m'}g(y,t)K(y,y')g(y',t)\,\mathrm{d}y' \\ & + \int_{y_0}^{\infty}\frac{m}{m'}Q(y,y')P(y')g(y',t)\,\mathrm{d}y' - \frac{1}{3m^2}g(y,t)P(y).\end{aligned} \tag{9}$$

To solve Eq. (9) numerically, we use a logarithmically equidistant mass grid,

$$m_{k+1} = \beta m_k, \quad k = 1,\ldots,n, \tag{10}$$

where β is an arbitrary number ($\beta > 1$) and n is the total number of bins for particle size spectrum. Thus, the y grid is equally spaced, $\Delta y_k = \ln r_{k+1} - \ln r_k = \ln\beta/3$. Typically, β is set to be $2^{1/x}$ with x is an integer. This yields a doubling of the particle mass after x bins. It has been shown that the increasing value of x decelerates the evolution of the floc spectrum (Bott, 1998). To achieve a reasonable compromise between numerical accuracy and efficiency, $\beta = 2^{1/4}$ is applied in the study.

As a result of the discretization, the collision of floc of mass m_i with floc of mass m_j will produce a new floc whose mass $m' = m_i + m_j$ which in general falls between m_k and m_{k+1}. To conserve particle mass a two-step procedure is used. In the first step, the newly formed floc with mass m' is added to grid box k. In the second step, an advection equation is solved to move a certain fraction, proportional to $(m'-m_k)/(m_{k+1}-m_k)$, of the floc mass from grid k to k+1. A higher-order positive definite advection scheme (Bott, 1989) is used to prevent numerical diffusion. A detailed description of the numerical implementation of the flocculation model is given in the Appendix A.

Winterwerp (1998) performed a settling column lab experiment to measure floc size variations with turbulent shear and SSC. Initially, a certain amount of particles with primary particle size ($D_p = 4\,\mu\mathrm{m}$) is placed into a cylinder where a homogenous turbulence field is generated through an oscillating grid. The particles are initially homogeneously mixed, and measurements are taken at the bottom when the system reaches equilibrium. Three test cases (T71, T69, and T73) with experimental parameters and results are listed in Table 1.

We carry out a flocculation simulation to verify the size-resolved method described above. Our simulation applies the same initial concentrations, shear rates, and primary particle size as in the experiments. Effects of differential settling on the aggregation rate are not considered, i.e., $K_{ds} = 0$.

We run the simulation until the floc size distribution reaches a dynamic steady state. The variations in median floc size (D_{50}) with time and the floc size distribution at steady state for the three tests are shown in Fig. 1. The floc size distributions at steady state (the lower panel of Fig. 1) show $D_{25}-D_{75} \approx 0.5D_{50}$, where D_{25} and D_{75} are the upper and lower quartile of floc size by mass. The median floc sizes are about 209, 199, and 157 μm at steady state, and the flocculation time scales (T_f), defined as the time scale for 95% of particles to reach their equilibrium values (Winterwerp, 2002), are about 6000, 900 and 200 s for test T71, T69 and T73, respectively. The model results are comparable with the experimental values (see Table 1 and Fig. 4 in Winterwerp, 1998).

Fig. 2 shows temporal evolution of the floc size distribution for the test case T69. At the beginning of the simulation, aggregation dominates and quickly shifts the flocs towards larger sizes. As the flocs become larger and more fragile, breakup becomes more important and starts to decelerate the growth of flocs. Finally, equilibrium between aggregation and breakup and a steady state of the particle size distribution is achieved. We note that the wiggles in the small floc size at $t = 300$ s in Fig. 2 are caused by the simulation starting with all particles in the first bin. At $t = 300$ s the simulation has not reached a steady state and there are some primary particles and small flocs left. We have conducted another simulation with an initial log–normal distribution of flocs, and the wiggles are eliminated (not shown).

To test the sensitivity of the model towards fractal dimension and particle stickiness, two sets of numerical experiments were done. For the first set, the fractal dimension (n_f) in the expression for the breakup frequency varies from 1.8 to 2.2, with the other settings the same as in the base case. The resulting median floc sizes are listed in Table 2 and show that the floc size increases as fractal dimension increases. The reason is that the increase of n_f reduces the breakup frequency (Eq. (3)), and allows the formation of larger flocs.

Table 1
Parameters and results in the three test cases (adopted from Winterwerp, 1998)

Test no.	C_0 ($\mathrm{g\,l^{-1}}$)	G ($\mathrm{s^{-1}}$)	D_{50} (μm)
T71	0.65	7.3	270
T69	1.17	28.9	241
T73	1.21	81.7	140

C_0 is the total mass concentration, G is the shear rate, and D_{50} is median particle size at equilibrium.

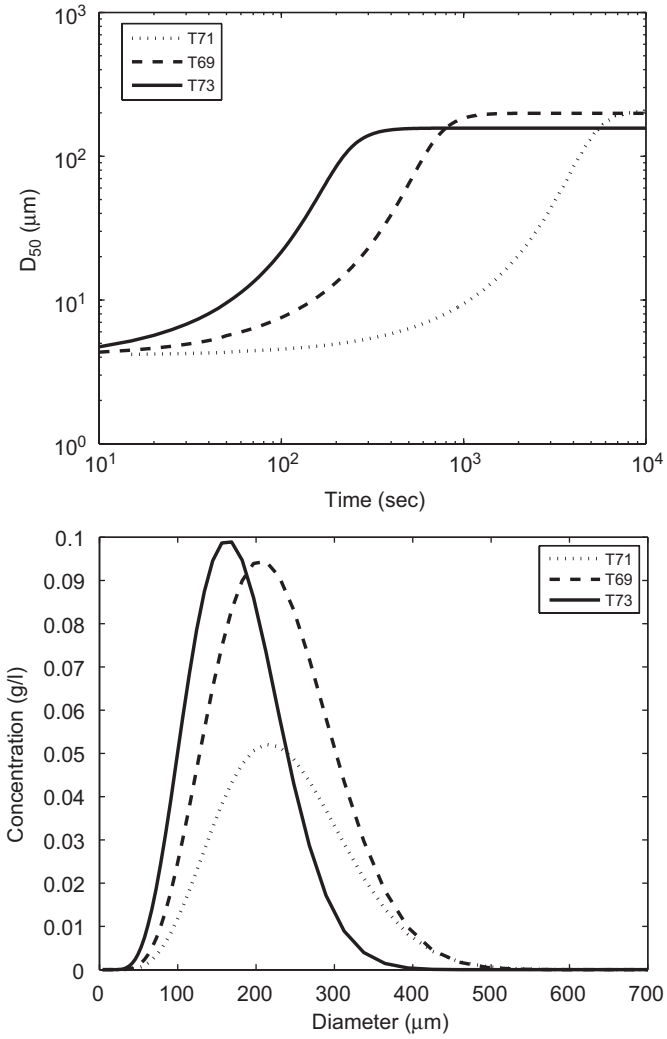

Fig. 1. Variations of median floc size (D_{50}) with time (upper panel), and floc size distributions at steady state (lower panel) for three test cases of flocculation simulation.

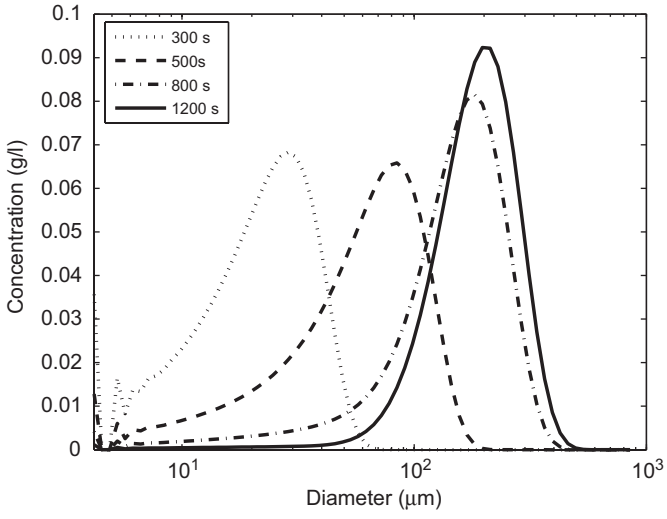

Fig. 2. Temporal evolution of floc size distributions for test case T69.

Table 2
The median floc size (μm) under different fractal dimension (n_f) simulations

Test no.	$n_f = 1.8$	$n_f = 1.9$	$n_f = 2.0$	$n_f = 2.1$	$n_f = 2.2$
T71	145	172	209	256	322
T69	139	165	199	245	307
T73	112	132	157	190	236

Table 3
The median floc size (μm) under different particle stickiness (α) simulations

Test no.	$\alpha = 0.05$	$\alpha = 0.1$	$\alpha = 0.2$	$\alpha = 0.4$	$\alpha = 0.7$	$\alpha = 1.0$
T71	56	80	113	158	209	249
T69	55	76	107	151	199	238
T73	43	60	85	119	157	187

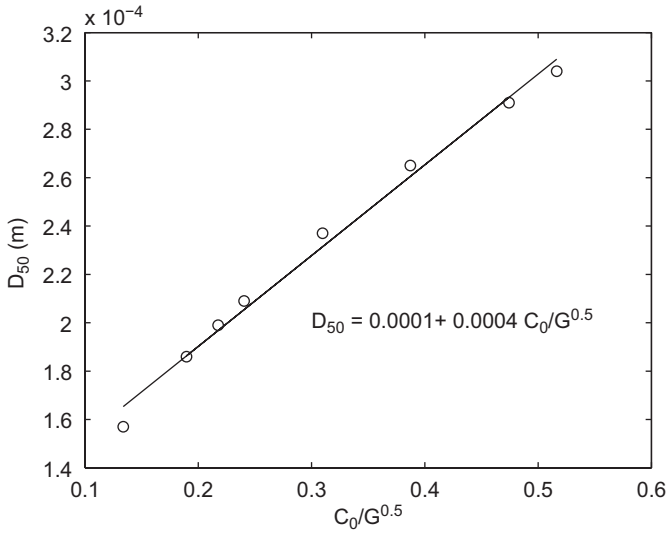

Fig. 3. Regression of median floc size (D_{50}) with $C_0/G^{0.5}$; the line indicates a linear regression fit ($\gamma^2 = 0.99$).

For the second set, the particle stickiness α is taken as 0.05, 0.1, 0.2, 0.4, and 1.0 with the other settings identical to the base case. Table 3 shows the results for the median floc size for different α values. The floc size generally increases with increased α. $D_{50} \propto \alpha^{0.5}$ is found using unconstrained nonlinear optimization ($\gamma^2 = 0.93$). Also, as α decreases, the flocculation time scale increases due to the longer time required to reach equilibrium.

Winterwerp (1998) proposed a relationship for the median floc size,

$$D_{50} = D_p + \frac{k_A C_0}{k_B \sqrt{G}}, \tag{11}$$

where k_A and k_B are aggregation and breakup coefficients, respectively, determined from fitting the experiment results. To evaluate this relationship with our model results, five additional model runs are completed with different values for $C_0/\sqrt{G}$ to increase the data range. Excellent regression ($\gamma = 0.99$) is obtained (Fig. 3). However, in our regression fit, the constant (D_p) is about 1×10^{-4} m, and the slope is about 4×10^{-4} m^4 kg^{-1} s$^{-0.5}$. From Winterwerp (1998), D_p is about 4×10^{-6} m, and the slope is about 4×10^{-3} m^4 kg^{-1} s$^{-0.5}$. In our simulation the particle size distributions are slightly skewed to the right (lower panel in Fig. 1). Thus the D_{50} is larger than the floc size in one-floc

approach in Winterwerp (1998) that assumes symmetrical distribution.

3. A 1-D sediment transport model

In the following section we investigate the interplay of flocculation processes with vertical transport. The governing equation for this 1-D simulation is

$$\frac{\partial g(y,t)}{\partial t} - \frac{\partial w_{s,i} g(y,t)}{\partial z} = \frac{\partial}{\partial z}\left(K_3 \frac{\partial g(y,t)}{\partial z}\right) + \text{flocculation}, \quad (12)$$

where z is the vertical dimension and K_3 is the vertical eddy diffusivity. Eq. (12) describes the change in the mass density distribution due to vertical transport and flocculation. Settling, turbulent diffusion and flocculation are considered, while vertical advection is ignored (small compared to settling). The flocculation term is as in Eq. (9). The eddy viscosity/diffusivity follows the Prandtl mixing-length theory, and the Prandtl Schmidt number is assumed to be unity. The diffusivity K_3 and turbulent dissipation rate ε are calculated (Orton and Kineke, 2001; Hill and McCave, 2001):

$$K_3 = \kappa u_* z(1 - z/H) \quad \text{and} \quad \varepsilon = u_*^3/\kappa z, \quad (13)$$

where κ is von Kármán's constant ($\kappa = 0.4$), and u_* is the friction velocity. The settling velocity $w_{s,i}$ is calculated from Eq. (7). The bottom erosion mass flux $E_{s,i}$ of particle in bin i is modified from Warner et al. (2005),

$$K_3 \frac{\partial g_i}{\partial z}\Big|_{bottom} = E_{s,i} = E_0\left(\frac{\tau_b}{\tau_c} - 1\right)\Big/ i, \quad \text{when } \tau_b > \tau_c \quad (14)$$

where E_0 is a bed erodibility constant. The bed shear stress $\tau_b = \rho u_*^2$, where ρ is the fluid density, 1010 kg m^{-3}. τ_c is the critical shear stress for erosion and is set to 0.12 Pa in the study (Righetti and Lucarelli, 2007). The constant $E_0 = 0.001$ kg m^{-2} s^{-1} is used (Ariathurai and Arulanandan, 1978). Eq. (14) is an empirical approach to account for the fact that larger particles are more difficult to erode than smaller ones. This is accounted for by the bin number i in the denominator. Eq. (12) is solved in two steps. First, the mass density function ($g(y,t)$) is updated at each vertical grid point via flocculation. Next, sedimentation and turbulent diffusion terms are applied on the vertical distribution of flocs of each bin.

The 1-D simulation results are compared with the observed size distribution over tidal cycles in a laboratory flume experiment of Bale et al. (2002). In the flume, oscillating currents are generated via a stirring plate. The current velocities range from 0.05 to 0.45 m s^{-1} over a period of 2 h, i.e., a full tidal cycle is 4 h. SSC and the particle sizes are measured. The experimental results show that SSC and median particle size vary periodically over the tidal cycles. Sediment erosion occurs when a critical velocity is exceeded. SSC increases quickly before the entire sediments are resuspended into the water column. The median size of particles is smallest near the minimum velocity, increases with erosion, but then decreases with the increasing of current velocity. As the velocity decreases, the median size of particles increases again, and SSC starts to decrease due to deposition.

We carry out model simulations of the flume experiment. The same parameters are used in both the simulation and experiment. The water column is 0.28 m deep, the initial SSC is 3520 mg l^{-1}, the primary particle size is 30 μm, and the density of the primary particles is 2650 kg m^{-3}. The lab experiments were carried out for different salinity, but the results are not sensitive. Our model simulation corresponds to salinity of 0.2 psu. We use 70 size bins to represent the particle size distribution, ranging from 30 to 1562 μm. The particle stickiness is 1.0. The sediment effects on

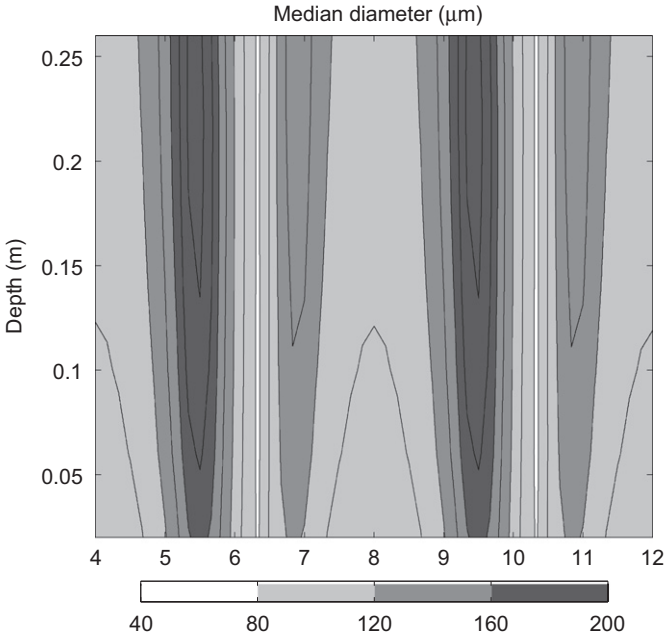

Fig. 4. Variations of median floc size (μm) with depth and time (hour) from 1-D simulation.

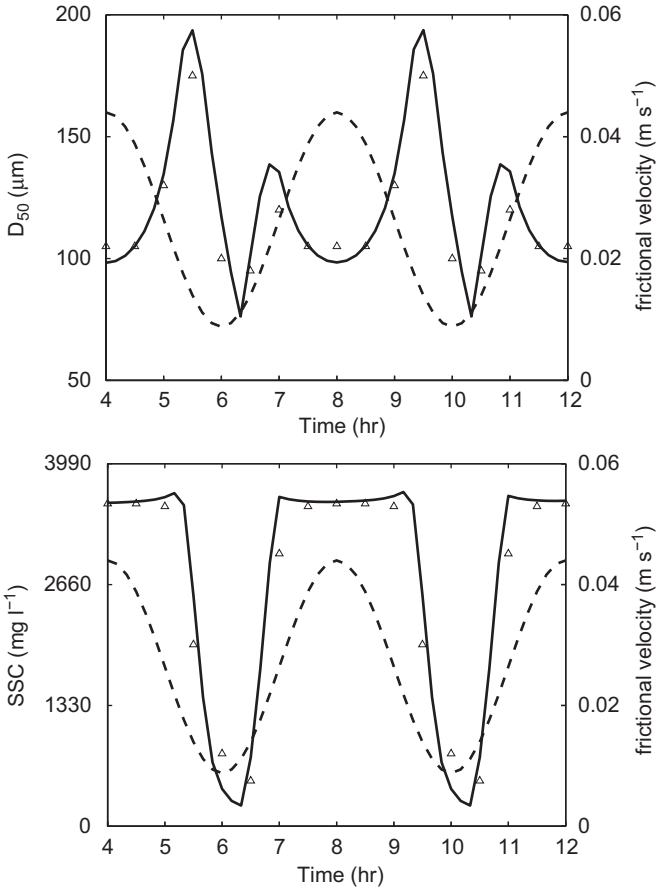

Fig. 5. Variations in floc size (solid line) over tidal cycles (upper panel) and variations in SSC (solid line) (lower panel) at 0.1 mab for 1-D simulation. The dash line is the frictional velocity, and the triangles are laboratory data adapted from Bale et al. (2002).

water density are ignored due to low SSC. Friction velocity is set to be sinusoidal cycles with a period of 4 h.

The simulation is integrated for three tidal cycles. Fig. 4 shows the contours of the floc median size in the water column during the last two tidal cycles. Typically, the floc size is smaller near the bottom due to the high turbulent level and dominant breakup process near the bottom. Fig. 5 compares the variations in floc size and SSC over the tidal cycles at the height of 0.1 mab (meter above bottom) between model simulation and lab experiment; the half hourly lab data are interpolated from Fig. 2 of Bale et al. (2002). The results of the model simulation are in good agreement with the experiment. The floc size is small during peak tidal currents even though SSC is high, due to the dominant breakup process caused by high turbulent shear. The floc size then starts to increase as tidal currents decrease, and reaches its maximum near slack tides due to dominant aggregation. After that, the floc size decreases rapidly due to preferential settling of large flocs coincident with an abrupt decrease of SSC. The floc size and SSC increase again when erosion occurs with the increased tidal currents.

The individual contributions to the temporal change of the floc mass density distribution ($\partial g/\partial t$) at hour 4.5 and 5.5 at 0.1 mab are separated to evaluate the effects of aggregation, breakup, diffusion, sedimentation, erosion and deposition on floc size variations (Fig. 6). The SSC is lower at hour 5.5 (Fig. 5), and hence, the magnitudes of $\partial g/\partial t$ are smaller at hour 5.5 than at hour 4.5. Fig. 6a shows that aggregation moves the mass from smaller sizes to larger sizes, while breakup has the opposite effect. The net effect of aggregation and breakup is shown in Fig. 6b. Production of large flocs ($D>100\,\mu m$) and depletion of small flocs ($D<100\,\mu m$) are observed at hour 4.5. As the aggregation proceeds, the maximum of the floc growth rate moves towards larger sizes as seen at hour 5.5. $\partial g/\partial t$ due to diffusion and sedimentation are shown in Fig. 6c. At hour 4.5, the mass of small flocs ($D<100\,\mu m$) increases due to a dominant upward diffusive flux, while the mass of large flocs ($100<D<200\,\mu m$) decreases due to a downward diffusive flux. At 0.1 mab, sedimentation contributes to the increase of large flocs ($D>150\,\mu m$). Thus, both diffusion and sedimentation contribute to the transport of large flocs towards the bottom where floc growth is mainly controlled by breakup processes. The simulation supports the hypothesis that the floc size throughout the water column can be limited by near-bed turbulence (Hill et al., 2001). The sum of the temporal changes by the above four processes indicates that the overall floc size increases at hour 4.5, but decreases at hour 5.5 (Fig. 6d). Erosion only occurs when the critical shear stress is reached. At hour 4.5, erosion and deposition rate balance each other at the bottom (Fig. 6e). At hour 5.5, the deposition rate increases because particles are mostly in the form of large flocs with high settling velocity.

The deposition rate describes the reduction of SSC throughout the water column with time. It is calculated in the lab experiment by fitting the observed concentration decline with time to an exponential function. In the laboratory experiment a deposition rate of $17.12\,g\,m^{-2}\,min^{-1}$ is obtained for an initial SSC of 3780 mg l^{-1} (Table 1 in Bale et al., 2002). The deposition rate calculated from the simulation is $19.47\,g\,m^{-2}\,min^{-1}$ using $d/dt\int c\,dz$ where c is local SSC and the integration is through the entire water column during the period when the total concentration decreases, e.g., from hour 5.5 to hour 6. Another simulation with initial SSC of $830\,mg\,l^{-1}$ is performed for further comparison. The calculated deposition rate is $4.46\,g\,m^{-2}\,min^{-1}$, which compares well with the experimental value of $3.31\,g\,m^{-2}\,min^{-1}$ (see Table 1 in Bale et al., 2002). These comparisons reinforce the model's fidelity in simulating of particle size and SSC variations.

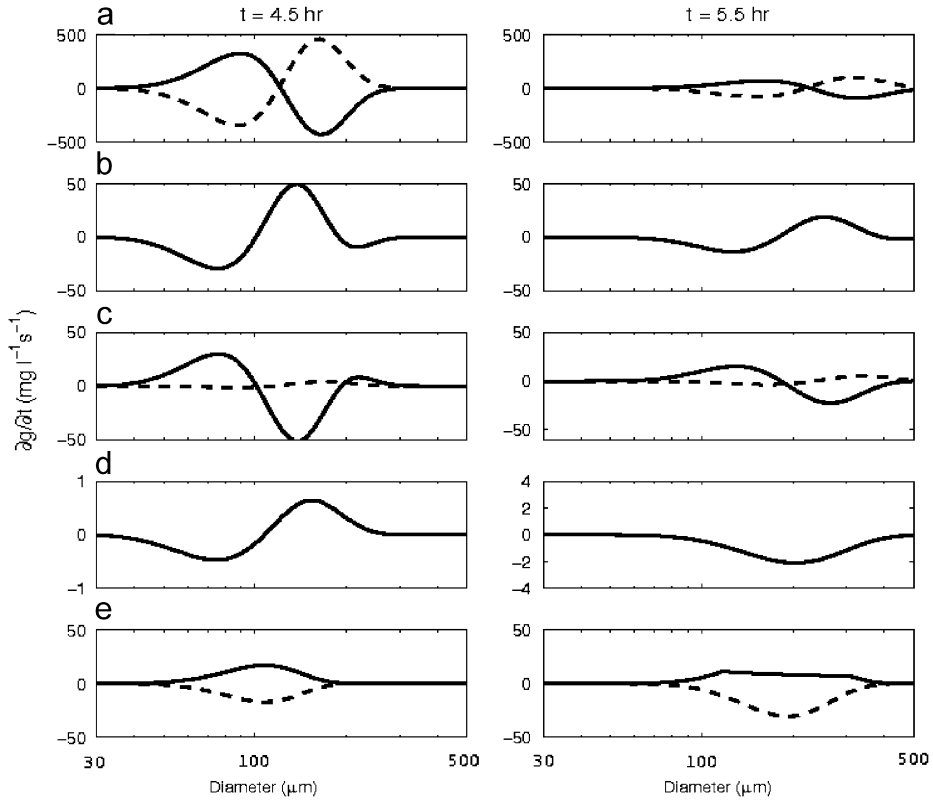

Fig. 6. The temporal changes of floc mass density distribution at 0.1 mab by (a) breakup processes (solid line) and aggregation processes (dash line), (b) the sum of changes by aggregation and breakup processes, (c) changes by diffusion (solid line) and sedimentation (dash line), (d) the sum of changes by the above four processes, and (e) by erosion (solid line) and deposition (dash line) at hours 4.5 (left) and 5.5 (right).

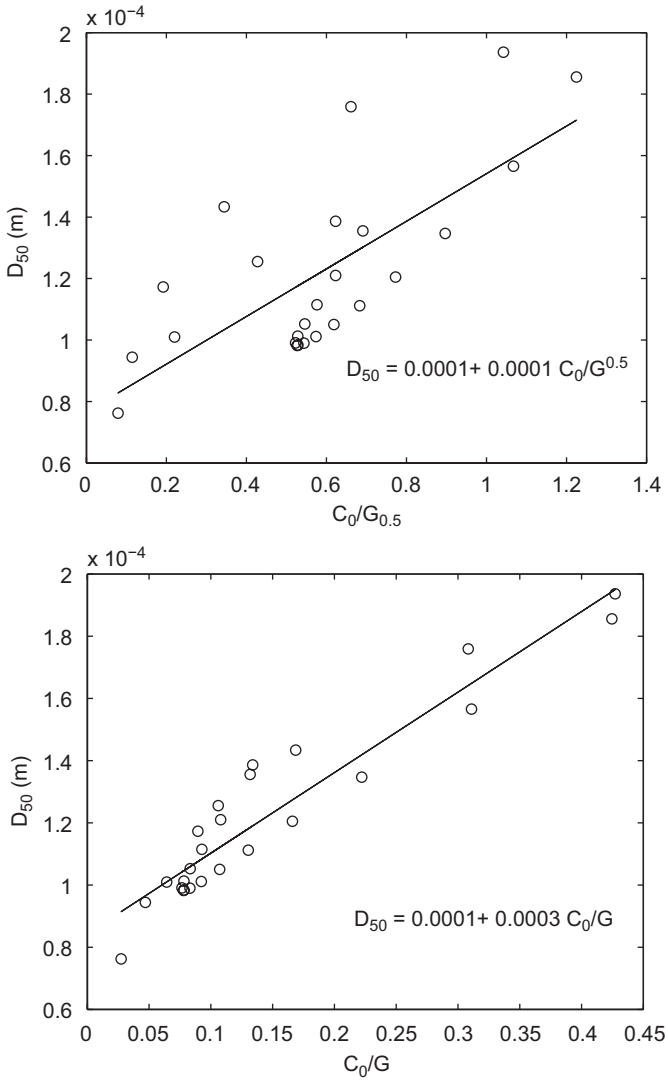

Fig. 7. Regression of median floc size (D_{50}) with $C_0/G^{0.5}$; the line indicates a linear regression fit ($\gamma^2 = 0.52$) (upper panel). Regression of median floc size (D_{50}) with C_0/G; the line indicates a linear regression fit ($\gamma^2 = 0.90$) (lower panel).

The simulation has shown that the floc size distribution changes depending on SSC and turbulent shear conditions. The relationship between median floc size, SSC and G can be explored (Fig. 7). In the previous study, we found that D_{50} is proportional to $C_0/\sqrt{G}$. For a regression fit for D_{50} and $C_0/\sqrt{G}$ of 1-D study we obtain a correlation coefficient $\gamma^2 = 0.52$. The decrease in correlation may be due to the 1-D floc sizes not in equilibrium, hence Eq. (11) is not valid. A much better regression, on the other hand, is obtained between D_{50} and C_0/G ($\gamma^2 = 0.90$), suggesting that the effect of turbulent diffusion is more important. Since $G = \sqrt{\varepsilon/\nu} = \nu/\lambda_0^2$, where λ_0 is the Kolmogorov microscale of turbulence, the inverse relationship between D_{50} and G is consistent with the observations that floc size is characterized by the Kolmogorov microscale (Fugate and Friedrichs, 2003).

A simulation without flocculation processes is carried out to highlight the effects of flocculation on sediment transport. For this simulation we need to specify the floc size, which is kept constant throughout the whole simulation. To create conditions that are comparable to the simulation with flocculation we use the tidally-averaged floc size of 138 μm. For a fair comparison of the simulations with and without flocculation, we also change back

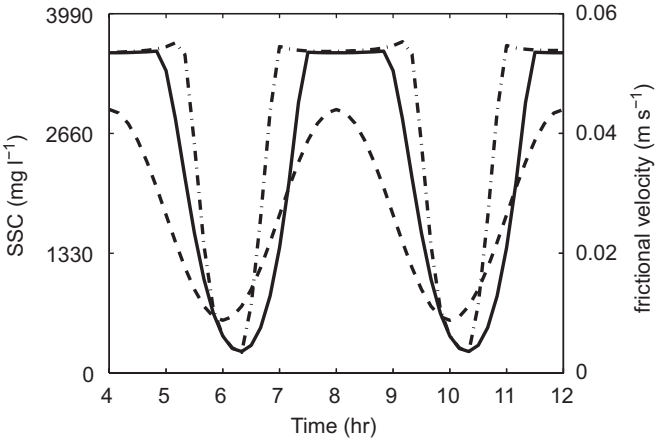

Fig. 8. Variations of SSC (solid line) and frictional velocity (dash line) of 1-D simulation without flocculation; SSC (dash-dotted line) with flocculation is included for comparison.

the bottom erosion flux to its original form,

$$E_{s,i} = E_0\left(\frac{\tau_b}{\tau_c} - 1\right), \quad \text{when } \tau_b > \tau_c, \tag{15}$$

where $E_0 = 5 \times 10^{-5}\,\mathrm{kg\,m^{-2}\,s^{-1}}$ and $\tau_c = 0.05\,\mathrm{Pa}$ (Warner et al., 2005). Fig. 8 shows variations in SSC with tidal currents at 0.1 mab. The maximum SSC is about $3520\,\mathrm{mg\,l^{-1}}$ during high tidal currents, and the minimum SSC is about $250\,\mathrm{mg\ l^{-1}}$ near slack tides. The timing difference between maximum current and SSC is due to the settling lag of particles (Friedrichs et al., 1998; Cheng, 2007). In both cases, all particles are eroded into the water column during maximum currents, hence, similar maximum SSCs are expected in the simulations with and without flocculation. Also, the constant floc size, 138 μm, is chosen to be the same as the averaged floc size from the case with flocculation. Thus, the same minimum SSCs are expected as both have the same averaged settling velocity. Simulation tests with a larger or smaller floc size cannot produce the expected SSC distribution. Hence, without the 'right' floc size, the simulation without flocculation will not produce the correct SSC. For these two scenarios (with and without flocculation) the difference comes from the variations in the settling velocity. Without flocculation the deposition rate during the time when the SSC declines sharply is only about 50% of that for the simulation with flocculation (Note the much sharper drop in SSC in the simulation with flocculation, Fig. 8.). With flocculation the floc size increases sharply as the currents decrease, whereas without flocculation the particle size remains the same.

Two sensitivity studies are performed to explore the effects of settling velocity and erosion rate on the floc size distribution and SSC. In the first numerical experiment, the settling velocity parameterization from Eq. (7) is replaced by a modified Stokes' law (Winterwerp, 2002),

$$w_{s,j} = \frac{2(\rho_s - \rho_w)g}{9\mu} \cdot r_1 r_j \tag{16}$$

where ρ_s and ρ_w are the densities of the primary particles and fluid, μ is dynamic viscosity of the fluid, 0.001 Pa S, and r_1 is the radius of primary particles. The results are similar to the base case, except that the maximum median floc size is slightly smaller, 160 μm versus 190 μm in the base case (not shown). For floc sizes <400 μm the settling velocity from Eq. (16) is larger than that from Eq. (7) (Fig. 9). The larger settling velocity contributes to a faster sinking of the flocs. As a result, the maximum floc size becomes smaller. Also, SSC is near zero near slack tides.

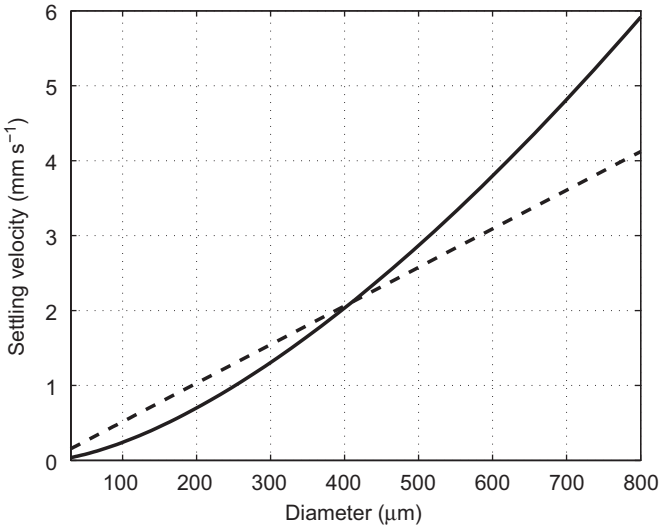

Fig. 9. The settling velocity of Sternberg et al. (1999) (solid line) and Winterwerp (2002) (dash line).

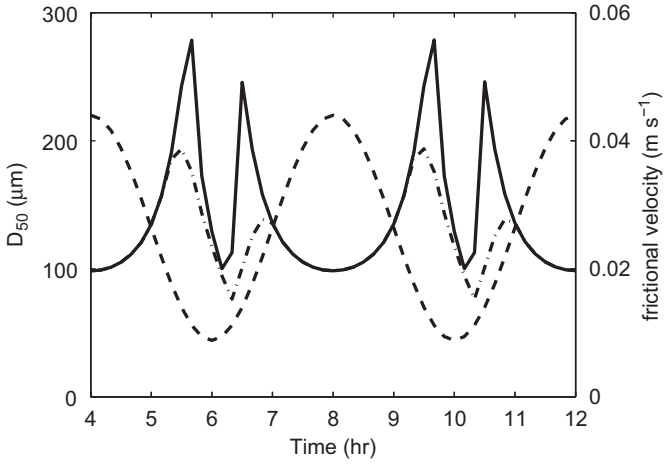

Fig. 10. Variations of medium floc size (solid line) and frictional velocity (dash line) over tidal cycles for 1-D simulation with the erosion flux of Warner et al. (2005); the median floc size of the base case (dash-dotted line) is included for comparison.

In the second experiment, the bottom erosion flux is changed to Eq. (15). All other settings are the same as in the base case. The variation patterns of the median floc size and SSC are qualitatively similar to the base case (Fig. 10). However, the maximum median floc size is much larger ~270 μm, due to the increase in erosion flux of the larger particles. Also, the secondary peak of the median floc size becomes more pronounced.

4. Discussions

We have developed a size-resolved flocculation model to simulate the variations in floc size and SSC distributions. The size-resolved model is evaluated with published laboratory measurements. The flocculation simulation results are comparable with Winterwerp (1998). Varying the particle stickiness indicates that the median diameter and stickiness are related by $D_{50} \propto \alpha^{0.5}$. Floc size variations over tidal cycles are simulated in the 1-D study in which sedimentation, diffusion, deposition and erosion are considered besides flocculation. The results are in good agreement with Bale et al. (2002). Analysis of the temporal changes of the floc mass density distribution shows the interplay of particle flocculation and vertical transport. The high turbulence intensity during the peak currents limits the maximum floc size. Diffusion and sedimentation influence the distribution of suspended particles in the water column. Large flocs are moved to the bottom and destroyed by intense near-bed turbulence. The competition between erosion and deposition controls the SSC. The study clearly demonstrates the need to include transport and flocculation simultaneously for sediment simulation.

The sensitivity test suggests that the floc formation is sensitive to the erosion flux and the availability of bottom sediments. Since most previous erosion model studies have dealt with a single particle size, it is not clear whether our simple generalization to a size-dependent erosion flux (Eq. (14)) is adequate in real world applications. The settling velocity formulation, on the other hand, does not appear to have significant effect for the floc size range considered in this study. For large aggregates ($D > 500$ μm) different settling velocity formulation could become critical.

In a study of the turbidity maximum in the upper reaches of the Tamar estuary, UK, Bass et al. (2007) and Manning et al. (2007) found that over a tidal cycle the maximum floc size was over 600 μm at SSC = 4.2 kg m^{-3} and $\tau = 0.38$ Pa, and decreased to about 220 μm at SSC = 0.04 kg m^{-3} and $\tau = 0.01$ Pa. The corresponding median floc size was about 380 and 150 μm (see Figs. 5 and 7 of Manning et al., 2007). Using the regression relationship (lower panel of Fig. 7) derived from our model simulations, we obtain the median floc size of 393 and 143 μm, respectively. Considering the large temporal variations of the median floc size, the excellent agreement with field observations is probably fortuitous.

The sediment transport modeling results are generally consistent with the observations of floc size in estuaries. Traykovski et al. (2004) described the suspended sediment size distribution at 1.5 mab over eight tidal cycles in the Hudson Estuary. On both flood and ebb tides, the particle size was small with means around 40 μm during maximum currents, but became significantly larger with means around 250 μm as currents decreased. Measurements of floc size in the turbidity maximum of the Ouse Estuary, UK, showed that near mid-depth the median floc size was about 500 μm at high water slack, but decreased to about 100 μm on the ebb and about 70 μm on the flood (Uncles et al., 2006). Estimates of floc size from the estimates of settling velocity in the York River Estuary suggested that the floc size was limited by the Kolmogorov microscale under peak tidal currents (Scully and Friedrichs, 2007). In the 1-D simulation, the floc size variation shows qualitatively the same temporal patterns with tidal currents as the observations. The size range, which depends on local tidal currents and total SSC, is different from the observations.

Acknowledgements

This study is supported by the New York Sea Grant Institute. The anonymous reviewers are gratefully appreciated for their helpful comments.

Appendix A. Description of the size-resolved flocculation model

The flocculation model solves two processes, aggregation and breakup.

A.1. Aggregation processes

For the treatment of the aggregation processes, we use the method by Bott (1998). The particle mass density function $g(y,t)$ is the prognostic variable. In discretized form, a change in the mass distributions g_i and g_j is calculated by the aggregation of flocs with mass m_i with flocs of mass m_j.

$$g_i(i,j) = g_i - g_i \frac{K(i,j)}{m_j} g_j \Delta y \Delta t, \tag{A1}$$

$$g_j(i,j) = g_j - g_j \frac{K(i,j)}{m_i} g_i \Delta y \Delta t, \tag{A2}$$

where g_i and g_j are the mass distribution functions at bin i and j before aggregation while $g_i(i,j)$ and $g_j(i,j)$ are the new mass distributions after aggregation. New flocs with mass m' ($m' = m_i + m_j$) are produced by aggregation of smaller flocs in bin i and j. The new mass distribution is the sum of the second term on the right hand side of Eqs. (A1) and (A2):

$$g'(i,j) = \frac{m'(i,j)}{m_i m_j} g_i K(i,j) g_j \Delta y \Delta t. \tag{A3}$$

However, usually the newly-formed m' is not fit in the pre-defined mass bins (Eq. (10)), and

$$m_k \leqslant m' \leqslant m_{k+1}. \tag{A4}$$

Then the mass density $g'(i,j)$ has to be split into bin k and k+1. A two-step procedure is applied to accomplish the partitioning. First, all $g'(i,j)$ is added to bin k and yields

$$g'_k(i,j) = g_k + g'(i,j). \tag{A5}$$

Second, a certain fraction of the new mass $g'(i,j)$ is moved to bin k+1. The distribution can be expressed as

$$\begin{aligned} g_k(i,j) &= g'_k(i,j) - f_{k+1/2}(i,j) \\ g_{k+1}(i,j) &= g_{k+1} + f_{k+1/2}(i,j). \end{aligned} \tag{A6}$$

$f_{k+1/2}(i,j)$ is the mass transported from bin k to k+1. A upstream scheme called upstream flux method (UFM) in Bott (1998) is used to calculate $f_{k+1/2}(i,j)$,

$$f_{k+1/2}(i,j) = c_k g'(i,j), \tag{A7}$$

where c_k is defined as

$$c_k = \frac{\ln(m'(i,j)/m_k)}{3\Delta y_k}. \tag{A8}$$

Note that $3\Delta y = 3(\ln\beta/3) = \ln\beta = \ln(m_{k+1}/m_k)$. Hence if c_k is about one, all new flocs go into bin k+1, otherwise only a percentage of new flocs is moved to bin k+1.

A.2. Breakup processes

In discretized form, the floc mass distributions due to breakup is updated by

$$\begin{aligned} g'_i &= g_i - P_i g_i \Delta t \\ g'_j &= g_j + P_i g_i \Delta t \end{aligned} \tag{A9}$$

where g'_i and g'_j are the floc mass density functions in bin i and j after breakup, and P_i is the breakup kernel defined in Eq. (3). We assume one large floc is broken up into two flocs with equal mass. According to Eq. (10) and $\beta = 2^{1/x}$, floc mass is doubling after every x bins. Thus the mass of broken-up flocs, is moved to bin $j = i - x$. The breakup procedure starts from flocs in bin $i = x$+1. The mass is transported to bin 1. In the next step, the broken flocs in bin $i = x$+2 is moved to bin 2. The calculation is continued until the breakup of the largest flocs.

The flocculation code is available by contacting the authors (fanxu@ic.sunysb.edu).

References

Ariathurai, C.R., Arulanandan, K., 1978. Erosion rates of cohesive soils. Journal of the Hydraulics Division, ASCE 104 (2), 279–282.

Bale, A.J., Uncles, R.J., Widdows, J., Brinsley, M.D., Barrett, C.D., 2002. Direct observation of the formation and break-up of aggregates in an annular flume using laser reflectance particle sizing. In: Winterwerp, J.C., Kranenburg, C. (Eds.), Fine Sediment Dynamics in the Marine Environment. Elsevier, Amsterdam, pp. 189–201.

Bass, S.J., Manning, A.J., Dyer, K.R., 2007. Preliminary findings of a study of the upper reaches of the Tamar Estuary, UK, throughout a complete tidal cycle: part I: linking hydrodynamic and sediment cycles. In: Maa, J.P.-Y., Sanford, L.P., Schoellhamer, D.H. (Eds.), Estuarine and Coastal Fine Sediments Dynamics—Proceedings in Marine Science, vol. 8. Elsevier, Amsterdam, pp. 1–14.

Bott, A., 1989. A positive definite advection scheme obtained by nonlinear renormalization of the advection fluxes. Monthly Weather Review 117, 1006–1015.

Bott, A., 1998. A flux method for the numerical solution of the stochastic collection equation. Journal of Atmospheric Sciences 55, 2284–2293.

Burd, A., Jackson, G.A., 1997. Predicting particle coagulation and sedimentation rates for a pulsed input. Journal of Geophysical Research 102 (C5), 10,545–10,561.

Cheng, P., 2007. Modeling sediment transport in estuarine environment: effects of tidal asymmetry, lateral circulation and sediment-induced stratification. Ph.D. Thesis, Stony Brook University, USA.

Dyer, K.R., Manning, A.J., 1999. Observation of the size, settling velocity and effective density of flocs, and their fractal dimensions. Journal of Sea Research 41, 87–95.

Eisma, D., Chen, S., Li, A., 1994. Tidal variations in suspended matter floc size in the Elbe river and Dollard estuaries. Netherlands Journal of Aquatic Ecology 28, 267–274.

Farley, K.J., Morel, F.M.M., 1986. Role of coagulation in the kinetics of sedimentation. Environmental Science and Technology 20, 187–195.

Friedrichs, C.T., Armbrust, B.D., de Swart, H.E., 1998. Hydrodynamics and equilibrium sediment dynamics of shallow, funnel-shaped tidal estuaries. In: Dronkers, J., Scheffers, M. (Eds.), Physics of Estuaries and Coastal Seas. Balkema, Amsterdam, pp. 315–327.

Fugate, D.C., Friedrichs, C.T., 2003. Controls on suspended aggregate size in partially mixed estuaries. Estuarine, Coastal and Shelf Science 58, 389–404.

Geyer, W.R., Hill, P.S., Kineke, G.C., 2004. The transport, transformation and dispersal of sediment by buoyant coastal flows. Continental Shelf Research 24, 927–949.

Hill, P.S., McCave, I.N., 2001. Suspended particle transport in benthic boundary layers. In: Boudreau, B.P., Jorgensen, B.B. (Eds.), The Benthic Boundary Layer: Transport Processes and Biogeochemistry. Oxford University Press, Oxford, pp. 78–103.

Hill, P.S., Nowell, A.R.M., 1995. Comparison of two models of aggregation in continental-shelf bottom boundary layers. Journal of Geophysical Research 100 (C11), 22,749–22,763.

Hill, P.S., Syvitski, J.P., Cowan, E.A., Powell, R.D., 1998. In situ observations of floc settling velocities in Glacier Bay, Alaska. Marine Geology 145, 85–94.

Hill, P.S., Milligan, T.G., Geyer, W.R., 2000. Controls on effective settling velocity in the Eel River flood plume. Continental Shelf Research 20, 2095–2111.

Hill, P.S., Voulgaris, G., Trowbridge, J.H., 2001. Controls on floc size in a continental shelf bottom boundary layer. Journal of Geophysical Research 106 (C5), 9543–9549.

Hunt, J.R., 1986. Particle aggregate breakup by fluid shear. In: Mehta, A.J. (Ed.), Estuarine Cohesive Sediment Dynamics. Springer, Berlin, pp. 85–109.

Kranck, K., Milligan, T.G., 1992. Characteristics of suspended particles at an 11-h anchor station in San Francisco Bay, California. Journal of Geophysical Research 97, 11,373–11,382.

Lavelle, J.W., 1993. A model for estuarine sedimentation involving marine snow. In: Mehta, A.J. (Ed.), Nearshore and Estuarine Cohesive Sediment Transport. Washington, DC, USA, pp. 148–166.

van Leussen, W., 1994. Estuarine macroflocs and their role in fine-grained sediment transport. Ph.D. Thesis, University of Utrecht, Netherlands.

Maggi, F., 2005. Flocculation dynamics of cohesive sediment. Ph.D. Thesis, Delft University of Technology, Netherlands.

Manning, A.J., Bass, S.J., Dyer, K.R., 2007. Preliminary findings of a study of the upper reaches of the Tamar Estuary, UK, throughout a complete tidal cycle: part II: in-situ floc spectra observations. In: Maa, J.P.-Y., Sanford, L.P., Schoellhamer, D.H. (Eds.), Estuarine and Coastal Fine Sediments Dynamics—Proceedings in Marine Science, vol. 8. Elsevier, Amsterdam, pp. 15–33.

Mikkelsen, O.A., Hill, P.S., Milligan, T.G., Chant, R.J., 2005. In situ particle size distributions and volume concentrations from a LISST-100 laser particle sizer and a digital floc camera. Continental Shelf Research 25, 1959–1978.

Orton, P.M., Kineke, G.C., 2001. Comparing calculated and observed vertical suspended-sediment distributions from a Hudson River Estuary turbidity maximum. Estuarine, Coastal and Shelf Science 52, 401–410.

Pruppacher, H.R., Klett, J.D., 1980. Microphysics of clouds and precipitation. D. Riedel Publishing Co., Boston, MA, USA.

Riemer, N., Wexler, A., 2005. Droplets to drops by turbulent coagulation. Journal of Atmospheric Sciences 62, 1962–1975.
Righetti, M., Lucarelli, C., 2007. May the shields theory be extended to cohesive and adhesive benthic sediments? Journal of Geophysical Research 112, C05039.
Scully, M.E., Friedrichs, C.T., 2007. Sediment pumping by tidal asymmetry in a partially mixed estuary. Journal of Geophysical Research 112, C07028.
Smoluchowski, M., 1917. Versuch einer mathematischen Theorie der Koagulationskinetik kolloider Lősunger. Zeitschrift fur Physikalische Chemie 92, 129–168.
Spearman, J.R., Roberts, W., 2002. Comparison of flocculation models for applied sediment transport modeling. In: Winterwerp, J.C., Kranenburg, C. (Eds.), Fine Sediment Dynamics in the Marine Environment. Elsevier, Amsterdam, pp. 277–293.
Spicer, P.T., Pratsinis, S.E., 1996. Coagulation and fragmentation: universal steady-state particle-size distribution. American Institute of Chemical Engineers 42 (6), 612–620.
Sternberg, R.W., Berhane, I., Ogston, A.S., 1999. Measurement of size and settling velocity of suspended aggregates on the northern California continental shelf. Marine Geology 154, 43–53.
Syvitski, J.P.M., Asprey, K.W., Le Blanc, K.W.G., 1995. In-situ characteristics of particles settling within a deep-water estuary. Deep Sea Research II 42, 223–256.
Traykovski, P., Geyer, W.R., Sommerfield, C., 2004. Rapid sediment deposition and fine-scale strata formation in the Hudson estuary. Journal of Geophysical Research 109, F02004.
Uncles, R.J., Stephens, J.A., Law, D.J., 2006. Turbidity maximum in the macrotidal, highly turbid Humber Estuary, UK: flocs, fluid mud, stationary suspensions and tidal bores. Estuarine, Coastal and Shelf Science 67, 30–52.
Warner, J.C., Sherwood, C.R., Arango, H.G., Signell, R.P., 2005. Performance of four turbulence closure models implemented using a generic length scale method. Ocean Modeling 8, 81–113.
Winterwerp, J.C., 1998. A simple model for turbulence induced flocculation of cohesive sediment. Journal of Hydraulic Research 36, 309–326.
Winterwerp, J.C., 2002. On the flocculation and settling velocity of estuarine mud. Continental Shelf Research 22, 1339–1360.
Zhang, J.J., Li, X.Y., 2003. Modeling particle-size distribution dynamics in a flocculation system. American Institute of Chemical Engineers 49, 1870–1882.